Development of a single loop EPR test method and its relation to grain boundary microchemistry for alloy 600

Vivekanand Kain [*], Yutaka Watanabe

Department of Machine Intelligence and Systems Engineering, Tohoku University, Aoba-Ku, Sendai 980 8579, Japan

Abstract

A single loop electrochemical potentiokinetic reactivation test method has been developed for alloy 600 that produces good passivation on all the surfaces, good etching during the reactivation scan and no appreciable pitting. It is able to quantify and discriminate between samples with a wide range of degree of sensitization. The Pa value correlates well with the minimum level of chromium in the depletion regions at the grain boundaries. It has been shown that the width of the attacked regions is much larger than the width of chromium depletion regions and it does not show any direct correlation with either depth or width or with a volume parameter of chromium depletion regions. It has been shown that the chromium carbides are not attacked during the test and that the intragranular regions attacked during the test are the sites of chromium carbides in the grain matrix. A modified Pa parameter is shown to be sensitive down to 7.5 wt% chromium in the depletion regions and indicates that the intragranular carbides have shallower depletion profiles than those at grain boundaries. Comparison of the results of the single loop and the double loop tests showed a good correlation. © 2002 Elsevier Science B.V. All rights reserved.

PACS: 81.65.K; 81.70.Yp; 82.80.Fk; 62.40.M

1. Introduction

The nickel-based alloy, alloy 600, has been commonly used as a tubing material in the steam generators (SG) of pressurized water reactors (PWRs) and in different components in boiling water reactors (BWRs). Alloy 600 is prone to intergranular corrosion (IGC) and intergranular stress corrosion cracking (IGSCC) in a number of environments [1–4]. The SG tubing in PWR is prone to IGSCC from the primary side, known as primary water stress corrosion cracking (PWSCC), and IGSCC, IGC, pitting and enhanced general corrosion from the secondary side of SG [5,6]. While the corrosion problems from the secondary side have been addressed by controlling the water chemistry and the design of the SG, the PWSCC continues to be a matter of concern for reactors still operating with mill annealed alloy 600 tubing. The material, environment and stress parameters that make alloy 600 prone to IGSCC in high temperature water have been established [7–10]. However, there exists no single model or mechanism that explains all the features of PWSCC and allows for the prediction of the crack propagation rate and remaining life of the SG tubing [9–11].

The IGSCC of sensitized stainless steels (SS) in BWRs has been well understood and is commonly explained by the slip-dissolution theory [12]. The propagation of deep cracks in SS is well predicted by this theory from the knowledge of the passivation rate at the bared crack tip and crack tip strain rate. The passivation rate at the bared crack tip depends on the solution conductivity, corrosion potential and grain boundary sensitization. The crack tip strain rate depends on the stress, stress intensity and material behavior. Therefore,

[*] Corresponding author. Present address: Materials Science Division, Bhabha Atomic Research Centre, Mumbai 400 085, India. Tel.: +91-22 559 5067; fax: +91-22 550 5151.

E-mail address: vivkain@apsara.barc.ernet.in (V. Kain).

the characterization of sensitization is an important step in predicting the propagation rate of deep cracks and to predict the susceptibility of SS to IGSCC in BWR environment. Quantification of the degree of sensitization (DOS) by electrochemical potentiokinetic reactivation (EPR) test has been extensively studied for austenitic SS. The results of the EPR tests have been correlated to the susceptibility of SS to IGSCC in BWR environment [13]. The susceptibility of austenitic alloys to IGSCC in various environments has been shown to be correlated to the minimum level of chromium in the depletion regions at the grain boundaries [14–17]. There has been some concern for SCC of nickel-based alloys in BWRs, with life prediction methods based on the slip-dissolution model being established [18].

While the mechanism of PWSCC is not yet clear, it has been shown that the susceptibility of alloy 600 to IGSCC depends on the amount of carbon in the alloy and the presence of carbides at the grain boundaries [19]. In a BWR environment, the susceptibility of alloy 600 to IGSCC depends on the minimum level of chromium in the depletion regions at the grain boundaries [1–4,17]. Therefore, development of EPR test methods for alloy 600 has found a focus with many researchers in last few years [17,18,20–23].

The EPR test offers a quantification of the DOS, is a relatively fast technique and is a non-destructive test compared to the time consuming immersion tests used to assess the susceptibility of austenitic alloys to IGC. There has been a difference of opinion on which parameter of the depletion region (the minimum level of chromium, the width of chromium depletion or both) influences the result of the EPR test [20,21,24,25]. Recent studies have shown [17,18,26] that an added advantage of the EPR test is that it allows for the correlation of the results with the minimum level of chromium in the depletion regions at the grain boundaries, thus providing a sound basis to correlate the EPR results with the susceptibility to IGSCC.

In this study, a single loop version of the EPR test has been developed for alloy 600. Heat-treated samples with variation in grain boundary chemistry (e.g. minimum level of chromium varying from 4.2 to 10.1 wt%, width varying from 60 to 410 nm) have been used. The aim is to establish a SL-EPR test method that produces good passivation on all the surfaces before the reactivation, good etching during the reactivation scan and no appreciable pitting. The developed test should be able to distinguish samples with a wide range of sensitization that are used in this study. Further it is attempted to show if the results of the EPR test show a direct correspondence to the minimum level of the chromium or width or the volume of the depletion regions. The results of the single loop test have been compared with the results of the double loop test developed by Angeliu et al. [18] using the same material and heat treatments.

2. Experimental

2.1. Material

The material and the heat treatments used in this study are the same as used in a previous study by Angeliu et al. [18] to develop the double loop EPR test for alloy 600. The chemical composition of the alloy 600 is shown in Table 1. The material was in the solution-annealed (SA) condition (solutionized at 1100 °C for 30 min and water quenched) before the sensitization heat treatments. The average intercept length of grains was 117 μm or an ASTM grain size of 3.35. An extensive characterization of grain boundary chemistry was done by analytical transmission electron microscopy and has been reported earlier [18]. A summary of the heat treatments and the resultant widths measured on one side of the grain boundary (full width at half maximum: FWHM and ω_{13}: width at a chromium level of 13 wt%) and the minimum level of chromium in the depletion regions for each heat-treatment is shown in Table 2.

2.2. Single loop EPR test method

The solution for the test, test temperature and the scan rate used in this single loop test were the same as used in the double-loop EPR test reported earlier [18] and are as follows: test solution: 0.01 M H_2SO_4 + 0.0001 M KSCN (deaerated), temperature: 30 ± 1 °C and scan rate: 0.5 mV/s.

2.3. Vertex potential

For development of the single-loop EPR test method, a total of six different vertex potentials ranging from +200 to +880 mV vs. saturated calomel electrode (SCE)

Table 1
Chemical composition of alloy 600 used in this study (wt%)

Element	C	S	Cr	Fe	Ni	Mn	Si
Wt%	0.063	0.002	14.69	7.19	76.7	0.36	0.37

Table 2
Summary of chromium depletion profile measurement [18]

Designation	Heat-treatment	Minimum Cr (wt%)	FWHM (nm)	ω_{13} nm
GB1A	SA + 621 °C/24 h	4.25 ± 0.37	60 ± 20	110
GB1B	1100 °C/0.50 h (SA)	–	–	–
GB1C	SA + 621 °C/150 h	8.01 ± 0.66	150 ± 75	215
GB1D	SA + 740 °C/0.25 h	6.27 ± 0.44	60 ± 30	110
GB1E	SA + 740 °C/1.9 h	6.59 ± 0.18	130 ± 30	200
GB1F	SA + 800 °C/0.35 h	7.45 ± 0.47	125 ± 40	185
GB1G	SA + 800 °C/0.35 h + 900 °C/0.17 h	10.13 ± 0.20	410 ± 100	440

SA: Solution annealed, FWHM: full width at half maximum, ω_{13}: width at Cr = 13 wt%. The FWHM and ω_{13} are as measured on one side of the grain boundary.

and hold time of up to 20 min were evaluated. For identifying the vertex potential, the sample with the most severe sensitization (minimum chromium level in the depletion region), namely GB1A, was used. The passivation current density at the vertex potential and then at the start of the reactivation was monitored. The microstructure of the sample after applying the vertex potential was examined using an optical microscope to identify the nature of attack.

2.4. SL-EPR tests on heat-treated samples

Under the determined test parameters, the SL-EPR test was conducted on all the heat-treated samples that are listed in Table 2. At least three measurements were carried out on each heat-treated sample and the standard deviation was determined. Before starting each test, the samples were polished to a finish of 1 µm by diamond paste. The samples were kept immersed in the test solution until a stable open circuit potential was achieved. The reactivation charge was measured from the reactivation scan and the grain boundary area was calculated assuming circular grains as per the formula [25]

$$A_{gbc} = 1.57A \, W/\ell^*, \qquad (1)$$

where A_{gbc} is the grain boundary area assuming circular grains, A is the sample area in cm^2, W is the width of attacked grain boundaries and ℓ^* is the average intercept length in cm. In all these calculations, the term W was taken to be 1 µm. The Pa parameter calculated using A_{gbc} is designated as Pa(c)

$$Pa(c) = Q/A_{gbc}, \qquad (2)$$

where Q is the reactivation charge during SL-EPR test.

It has been suggested in earlier studies on austenitic SS [24,25] that instead of either the width or the minimum level of chromium of the depletion regions, a volume parameter may control the extent of attack during the EPR test. Therefore, a volume parameter (VP) was calculated using the equation

$$VP = \pi(\omega_{13})^2 \ell_{gb} C_{eff} \{(13.0 - Cr)/100\}, \qquad (3)$$

where ω_{13} is the width of the depleted regions at Cr = 13.0 wt% on one side of the grain boundary, ℓ_{gb} is the grain boundary length per unit sample area (=1.57 A/ℓ^*, A is 1 cm^2), C_{eff} is the total effective coverage (i.e. the length of the attacked regions at grain boundaries and the effective length of the intragranularly attacked regions, as a ratio of the grain boundary length) and Cr is the minimum level of chromium in the depleted regions at grain boundaries.

2.5. Microstructural characterization after SL-EPR test

The microstructure developed after the SL-EPR test was examined using a field emission-scanning electron microscope. For each sample, the amount of attacked grain boundary length, as a percentage of the total grain boundary length, as well as the maximum width of grain boundary attack was measured using image analysis (IA). The intragranular attack was also quantified as a percentage to the total attacked regions and designated as A_{GC}. Since all the heat-treated materials showed intragranular attack, energy dispersive spectroscopy (EDS) was conducted to identify the sites of these attacked regions. The EDS analysis was carried out on the GB1A sample and elemental mapping for chromium was carried out.

3. Results and discussion

3.1. Vertex potential for SL-EPR

The parameters like the scan rate, solution composition, KSCN concentration and test temperature have already been examined in detail by others [17,18] for the DL-EPR test for alloy 600. Using the conditions optimized in these studies [17,18], the vertex potential and the hold time were optimized for the SL-EPR test to develop good passivity on the most severely sensitized

Table 3
Effect of different vertex potentials on passivation current density

Vertex potential (mV vs. SCE)	Hold time (min)	Passivation current (μA/cm^2)	Passivation/ localized attack
+880	1	400	Localized attack
+700	10	3	Passivation
+600	10	17	Passivation
+600	20	15	Passivation
+400	10	15	Passivation
+200	10	12	Localized attack

sample. The overall aim is to allow for good passivity before a reactivation from the depleted grain boundaries and absence of any pitting during the test.

The passivation current density measured at different vertex potentials and hold times are listed in Table 3. The examination of the exposed surfaces after application of vertex potentials was done using an optical microscope and the results are listed in the same table. It is clear from this table that a potential of +700 mV (SCE) for 10 min provides the best passivation on the surfaces. This was further confirmed by measuring the passivation current density during the scan to the open circuit potential. The current density at the time of start of the reactivation was minimum when the vertex potential used was +700 mV (SCE). There was no appreciable improvement in the passivation current density when longer hold times were used at this vertex potential. There were clear localized attacks in the grains at the vertex potentials of +880 mV (SCE) and +200 mV (SCE). These two potentials were thus on the transition stages of passivity for alloy 600 under the test solution and conditions used in this study. Based on these results, a vertex potential of +700 mV (SCE) for 10 min was chosen for the SL-EPR test.

3.2. Results of the SL-EPR test on heat-treated samples

The final parameters of the SL-EPR test developed in this study are listed in Table 4. The average Pa values

Table 4
Test parameters of SL-EPR test

Test solution	0.01 M H_2SO_4 + 0.0001 M KSCN (deaerated)
Temperature	30 $\pm$ 1 °C
Surface finish	1 μm
Vertex potential	+700 mV (SCE)
Hold time	10 min
Scan rate	0.5 mV/s

Table 5
Results of the SL-EPR test and the microstructural characterization after the EPR test

Designation	Pa(c) (C/cm^2)	Coverage (at grain boundary) (%)	Intergranular attack, A_{GC},[a] (%)	Maximum attacked width (μm)
GB1A	71.25 $\pm$ 2.25	100	46.1	10.3
GB1B	0.12 $\pm$ 0.04	–	–	–
GB1C	39.5 $\pm$ 6.3	64.6	22.4	11.0
GB1D	48.0 $\pm$ 0.90	96.7	15.2	9.1
GB1E	46.6 $\pm$ 1.9	77.3	11.5	8.9
GB1F	33.8 $\pm$ 1.2	54.6	12.5	9.0
GB1G	12.0 $\pm$ 0.8	41.7	27.2	9.8

[a] Area of intragranularly attacked regions as percentage of the total attacked area.

and their standard deviations calculated from three measurements are listed in Table 5. The results of the IA for microstructural characterization after EPR testing are also shown in Table 5. The 'Coverage' is measured as the length of the attacked regions at the grain boundaries as a percentage of the grain boundary length. The C_{GC} is the effective length of the intragranularly attacked regions as a percentage of the grain boundary length. The C_{GC} is calculated assuming that the area fraction and the length fraction of the intragranularly attacked regions is equal. Therefore, C_{eff} can also be calculated as (Coverage + C_{GC})/100. The calculated values of C_{eff} and the volume parameter as per Eq. (3) are shown in Table 6. The microstructures of the samples after the EPR test

Table 6
Calculation of VP, Pa(gbc) and modified Pa(c) after the SL-EPR test

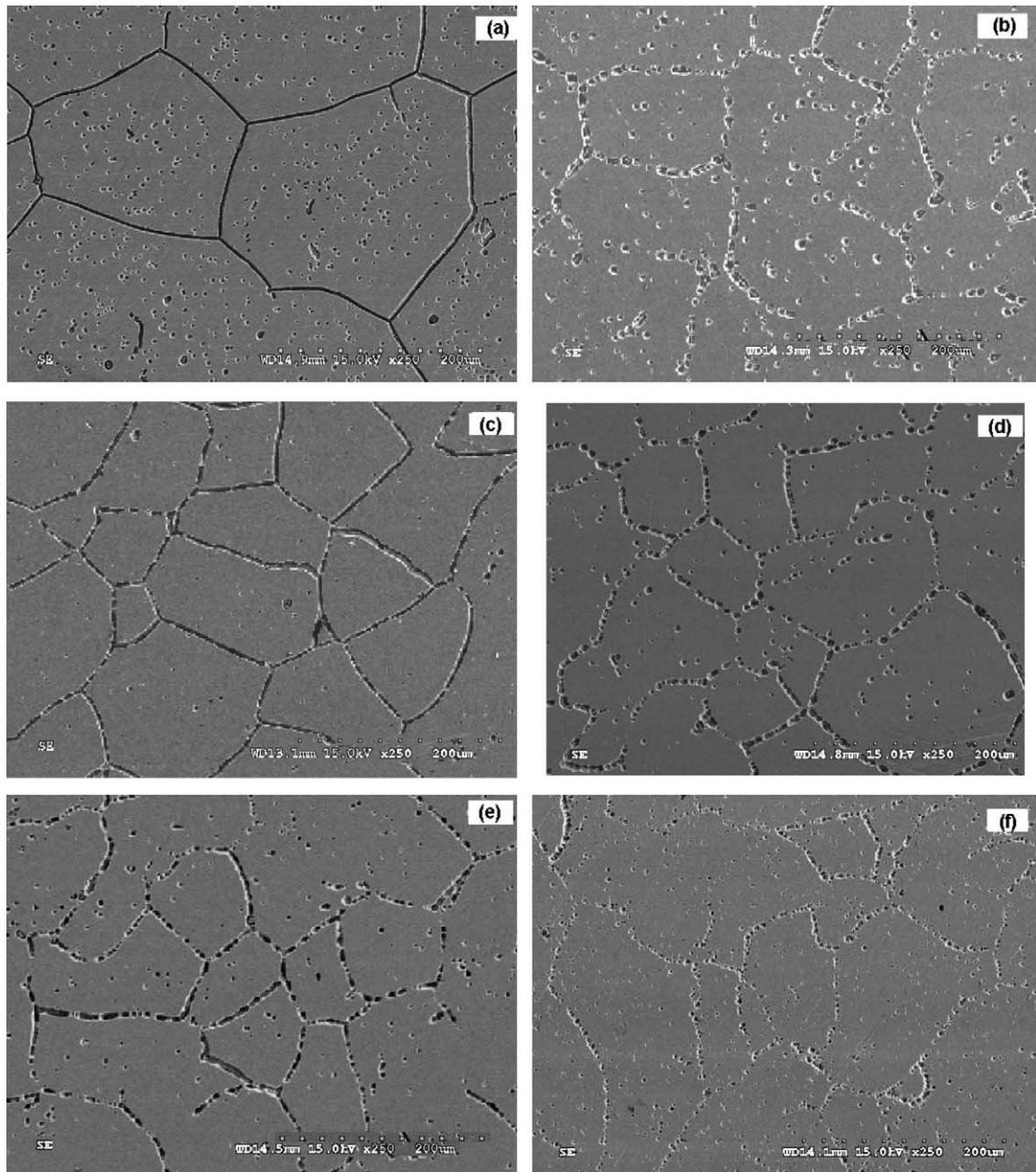| Designation	C_{GC} (%)	C_{eff}	VP ($\times 10^{-12}$) arbitary units	Pa(gbc) (C/cm^2)	Modified Pa(c) (C/cm^2)
GB1A	85	1.85	8206	38.51	38.51
GB1B	–	–	–	–	–
GB1C	18	0.83	8112	30.65	47.42
GB1D	17	1.14	3894	40.70	42.10
GB1E	10	0.87	9417	41.24	53.38
GB1F	8	0.62	4949	29.57	54.17
GB1G	16	0.57	13088	8.74	20.94

Fig. 1. The structure of the samples (a) GB1A (SA + 621 °C/24 h), (b) GB1C (SA + 621 °C/150 h), (c) GB1D (SA + 740 °C/0.25 h), (d) GB1E (SA + 740 °C/1.9 h), (e) GB1F (SA + 800 °C/0.35 h) and (f) GB1G (SA + 800 °C/0.35 h + 900 °C/0.17 h) after SL-EPR test.

are shown in Fig. 1(a)–(f). A typical microstructure that was used to measure the maximum width of attacked regions at the grain boundaries is shown in Fig. 2. In this figure the unattacked chromium carbides are clearly visible inside the attacked regions at the grain boundaries.

3.3. The EDS analysis on tested sample

Results of EDS analysis conducted on the sample GB1A (SA + 621 °C/24 h) after the EPR test is shown in Fig. 3. It is clear from the chromium map that the regions where the attack occurred at the grain boundaries
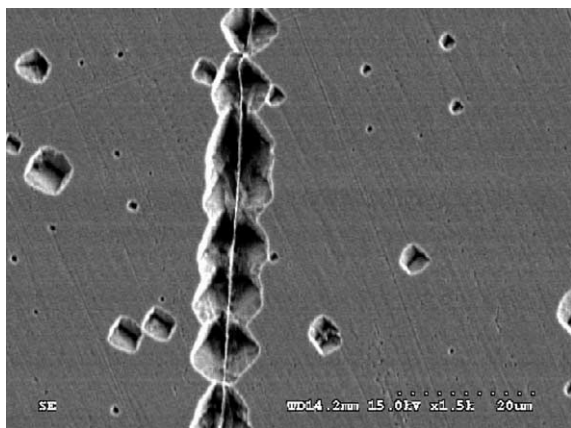
Fig. 2. The maximum width of attack in sample GB1C (SA + 621 °C/150 h) after the SL-EPR test. The unattacked chromium carbides are visible inside the attacked regions at the grain boundary.

as well as inside the grains are the regions that are adjacent to the chromium rich regions. It is thus evident that the attack occurred during the EPR test on the chromium-depleted regions adjacent to the chromium rich carbides. This EDS analysis showed that during the EPR test the chromium carbides are not attacked and remain inside the attacked regions even after the test. The direct observation of carbides after the EPR test has been reported for austenitic SS [27] and it has also been shown by EPR tests on desensitized samples of SS that the carbides do not dissolve during EPR test [28]. It is possible that many of these carbides fall out from the grain boundaries or from their intragranular positions due to wide attack on the surrounding chromium depleted regions. These results showed that the EPR test method developed in this study does not result in pitting attack in the grains and only the chromium depleted regions (at the grain boundaries and inside the grains) are attacked during the test.

3.4. Correlation of Pa parameter with grain boundary microchemistry

The Pa values are plotted against the minimum level of chromium in the depletion regions in Fig. 4(a) and against the full width at half maximum (FWHM) of the chromium depletion regions at the grain boundaries in Fig. 4(b). It is clear from Fig. 4(a) that there is a direct relationship between the minimum level of chromium in the chromium depletion regions and the parameter Pa. The higher the value of the minimum level of chromium in the depletion region, the lower is the Pa value. It is to be noted that the sample GB1C has the highest variation in the minimum level of chromium in the depletion regions (± 0.66 wt%) and this had resulted in maximum

variation in the Pa(c) values (± 6.3 C/cm^2) causing a small hump in Fig. 4(a). On the other hand, there is a good negative correlation between the FWHM of the chromium depletion regions and the Pa, as seen in Fig. 4(b). In this case, the larger the width of the depletion regions, the lower is the Pa value. This is contrary to the expectation of higher attack on wider depletion regions. This indicates that the width of the depletion regions does not influence the results of EPR test whereas the attack during EPR test is controlled mainly by the minimum level of chromium in the depletion regions. This is also reflected in the small peak observed in Fig. 4(b). The peak is observed because of an increase in the Pa(c) value from 33.8 C/cm^2 for the sample GB1F to 46.6 C/cm^2 for the sample GB1E in spite of only a small increase in their FWHM from 125 ± 40 nm to 130 ± 30 nm. The increase in the Pa(c) value for the sample GB1E is due to a lower level of chromium (6.59 wt%) than in the sample GB1F (7.45 wt%) though the two samples have essentially the same FWHM.

The volume parameter calculated using Eq. (3) was plotted with the Pa values in Fig. 4(c). It is evident that the Pa parameter does not have a direct correspondence with the volume parameter. This is due to the fact that the volume parameter contains the terms, width and the minimum level of chromium in the depletion regions, whereas these two parameters have different correlation with the Pa parameter as shown in Fig. 4(a) and (b). The deep but narrow chromium depletion profile as in sample GB1A has shown higher DOS (the Pa value) than the wide but shallow profiles as in sample GB1G.

3.5. Maximum width of attacked regions

In the EPR tests for SS, it had been shown that the width of attack is much greater than the width of the chromium depletion regions [25,26]. This was also clearly demonstrated in this study for alloy 600. While the width (FWHM) of the chromium depletion regions is in the range of 60–410 nm, the maximum width of the attacked regions in the EPR tests is in the range of 8.9–11 μm. In order to check if any correlation exists among the minimum level of chromium, the width of chromium depletion regions and the maximum width of attack in the EPR test, the maximum attacked width in the EPR test is plotted with the minimum level of chromium in the depletion regions in Fig. 5(a) and with FWHM in Fig. 5(b). It is clear that there exists no correlation between the minimum level of chromium or the width of the depletion regions with the maximum width of attack in the EPR test.

The maximum attacked width in the EPR test plotted against the volume parameter calculated as per Eq. (3) is shown in Fig. 5(c). There is no obvious correlation between the maximum attacked width in the EPR test and the volume parameter.
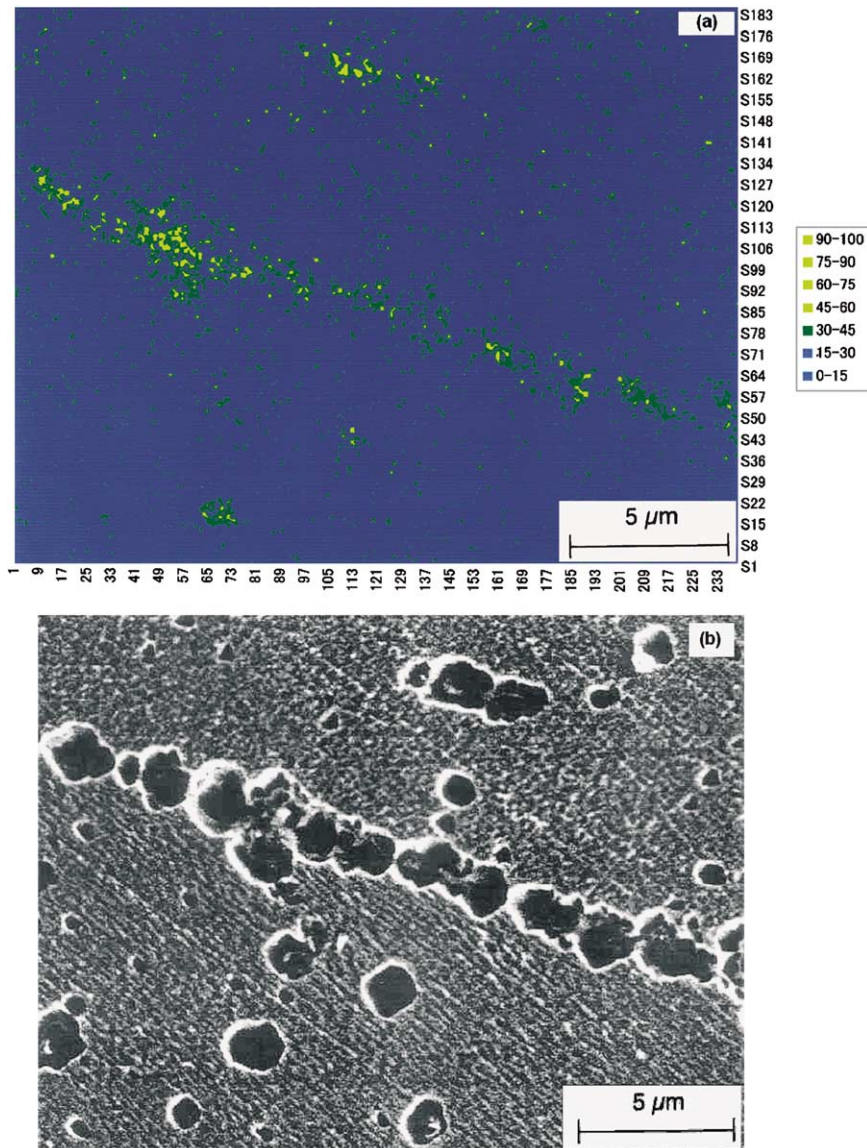
Fig. 3. (a) The chromium map and (b) the secondary electron image of the attacked region on sample GB1A (SA + 621 °C/24 h) after the SL-EPR test showing undissolved chromium carbides.

It is reported [25] that Cr^{+6} forms in the attacked regions increasing the severity of the solution inside the attacked regions. The lack of any clear correlation of the attacked width of the depletion regions in the EPR test is attributed to the fact that the solution inside the attacked regions, at the chromium depletion regions, is highly aggressive even to the undepleted regions next to the depleted regions [25]. Therefore, after the attack on the depleted regions the attack continues on the undepleted regions. The total time of the test (therefore the scan rate), the temperature and severity of the test solution determine the extent of attack. It has been shown

[25] that in 0.5 M H_2SO_4 + 0.01 M KSCN solution, the extent of attack depends upon the test temperature and it shows an Arrhenius relationship with the test temperature. Therefore, the severity of the solution within the attacked regions is expected to depend on the minimum level of chromium in the depletion regions. However, when the solution inside the attacked regions is highly aggressive, the attack at and adjacent the chromium depleted regions is severe and mainly influenced by the test temperature, the test duration and the test solution. This is why the maximum width of attacked regions in differently sensitized samples is large
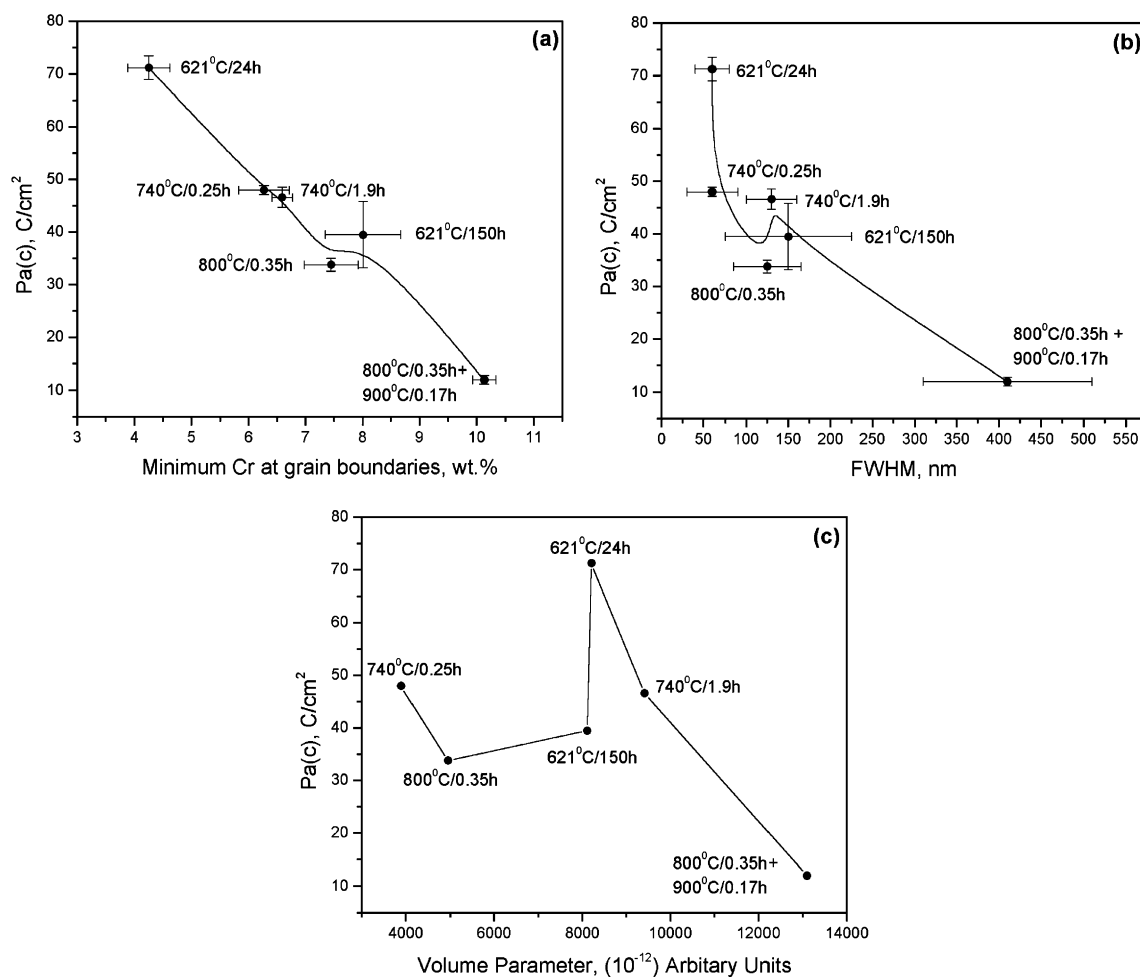
Fig. 4. Comparison of the Pa values measured from the SL-EPR test with (a) the minimum level of chromium [18], (b) the FWHM values [18] and (c) the volume parameter of the chromium depletion regions.

and in a narrow range of 8.9–11 μm. For SS, the widths of chromium depletion regions of the order of 10 nm have been reported [25,26] to have resulted in maximum attacked widths of 3–5 μm.

3.6. Single loop and double loop EPR tests

The results of the DL-EPR using the same material, heat-treatments, test solution, test temperature and scan rates were reported by Angeliu et al. [18]. In that study, a direct relationship was found between the minimum level of chromium in the depletion regions and the DL-EPR ratio. The EPR ratios in the DL-EPR test on the samples with the same heat-treatments are plotted against the Pa values in the SL-EPR test in Fig. 6. It is seen that there is good correlation between the two versions of the test. The wide range of the SL-EPR test results (Pa parameter) makes it more sensitive to dis-

criminate small differences in DOS. This is evident from the observation that the SL-EPR ranks sample GB1E (SA + 740 °C/1.9 h), with 6.59 wt% chromium in the depletion regions, as having higher DOS than sample GB1C (SA + 621 °C/150 h), with 8.01 wt% chromium in the depletion regions. It is to be noted that the width of the depletion regions in both the samples is almost the same. However, the DL-EPR test had ranked GB1C (SA + 621 °C/150 h) as having slightly higher DOS than GB1E (SA + 740 °C/1.9 h). This could be due to the large amount of intragranular attack in GB1C. It is also to be noted that the SL-EPR test takes less time than the DL-EPR test though it generally requires very good surface finish. The DL-EPR test is easy to carry out as it requires measurement of the peak current only and is also sensitive to the grain size, while in the SL-EPR test the sample area and the reactivation charge have to be measured. Hanninen et al. had also reported
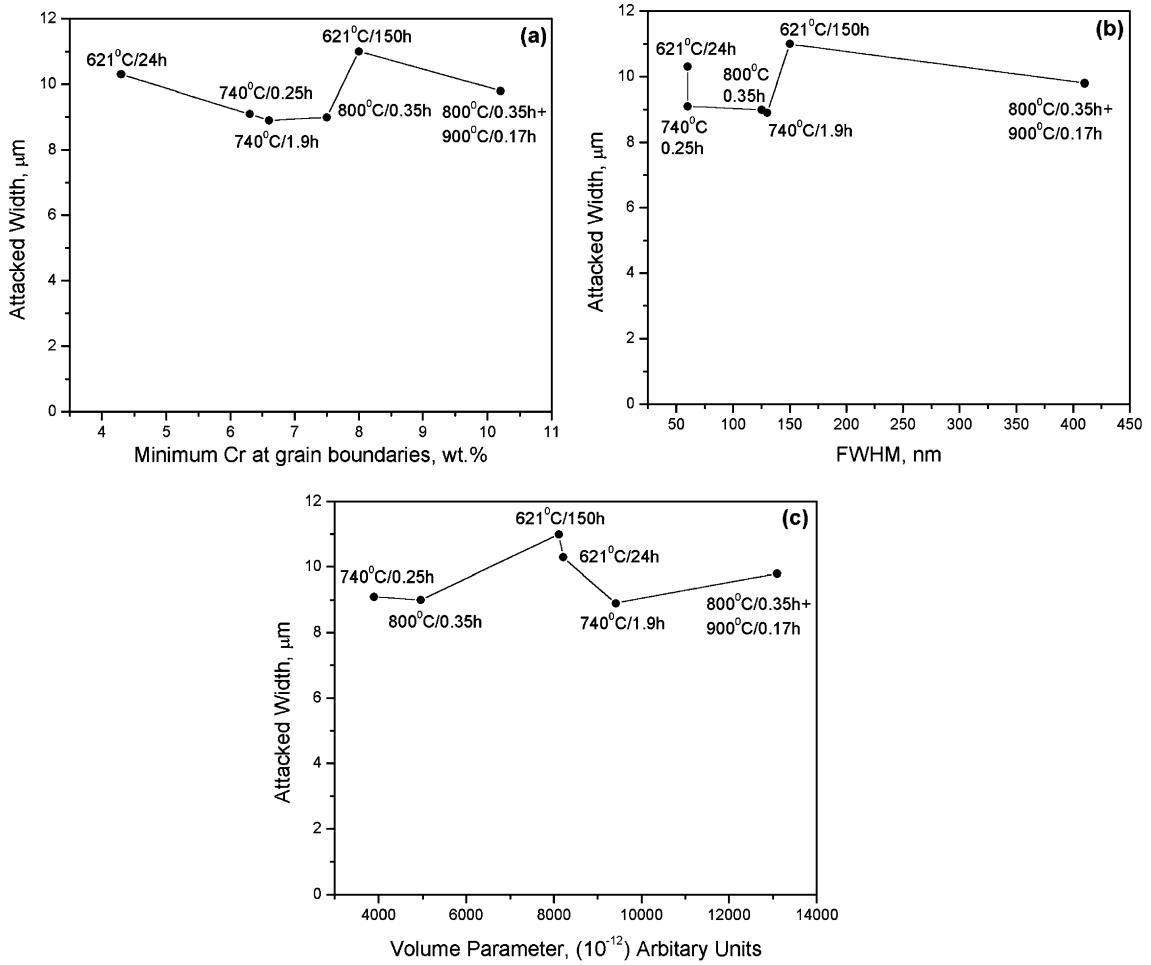
Fig. 5. The maximum attacked width after the SL-EPR test versus (a) the minimum level of chromium [18], (b) the full width at half maximum [18] and (c) the volume parameter of the chromium depletion regions.
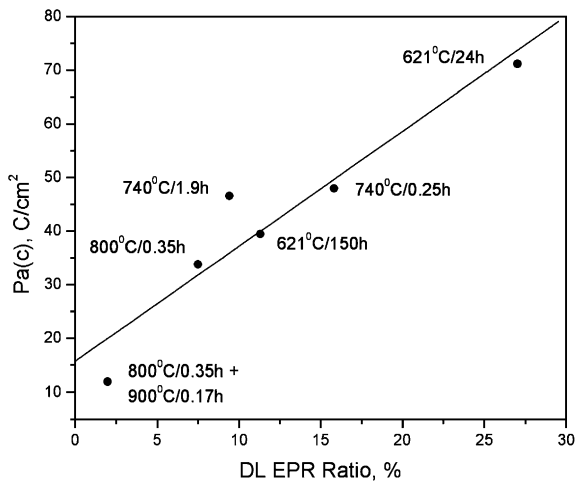

Fig. 6. The comparison of the results of the DL-EPR [18] and the SL-EPR tests.

[25] a good and similar correlation between the results of the single loop and the double loop EPR tests on type 304 SS. The interpretation of the Pa parameter in SL-EPR test gives more insights into the chromium depletion regions as shown in the Section 4.

3.7. SL-EPR test to determine the minimum level of chromium

It has been reported [26] that the SL-EPR test can be used to determine the minimum level of chromium in the grain boundaries. Since the Pa parameter is calculated with the assumption that all the grain boundaries contribute to the reactivation charge, the determination of the minimum chromium level is often difficult. The Pa parameter has to be modified [26] to take into account the actual coverage of the chromium depletion regions in the sample. The IA allows determination of the actual

coverage of the attacked regions in the test and it has been reported in Table 5. Since there are intragranular carbides in the material used in this study, it is assumed that the same charge density is emitted during the dissolution of the depleted regions at the grain boundaries and within the grains. When the reactivation charge from the intragranular carbides is subtracted, the Pa value obtained is the reactivation charge from the depleted regions at grain boundaries only per unit grain boundary area assuming that all the grain boundaries contribute to reactivation. This is designated as Pa(gbc) and is calculated as

$$\text{Pa(gbc)} = \text{Pa(c)}(1 - A_{\text{GC}}/100). \quad (4)$$

However, the reactivation comes from the grain boundaries actually covered by the depleted regions. Therefore, Pa(gbc) is divided by the actual (i.e. effective) coverage of the grain boundaries by the depleted regions. This gives the charge per unit attacked grain boundary area and should be a measure of the minimum level of chromium in the depleted regions as it is the only factor influencing the results of the EPR test. The modified Pa(c) can be calculated as follows:

$$\text{modified Pa(c)} = \text{Pa(c)}/C_{\text{eff}} = \text{Pa(gbc)}/(\text{coverage}/100). \quad (5)$$

The Pa(gbc) and the modified Pa values thus calculated have been shown in Table 6 and plotted against the minimum level of chromium in the depletion regions in Figs. 7 and 8. Fig. 7 shows that when the contribution of the intragranular carbides is subtracted, the Pa value saturates as the minimum chromium drops below 6.6 wt%. When the Pa value is calculated taking the actually attacked areas at grain boundaries, Fig. 8 shows that
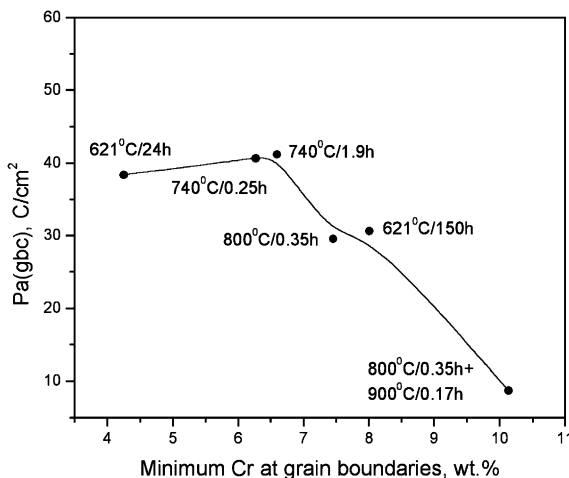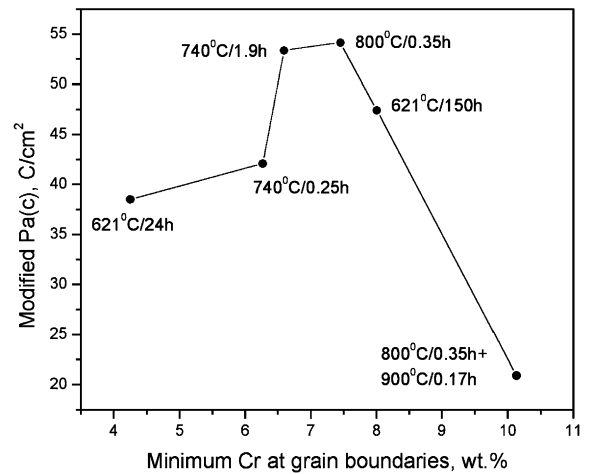

Fig. 8. Modified Pa parameter versus the minimum level of chromium [18] in the depletion regions.

down to 7.5 wt% there is a direct correlation between the modified Pa(c) and the minimum levels of chromium in the grain boundaries. However the modified Pa(c) values saturate at chromium levels below 7.5 wt% and have decreased for samples GB1A and GB1D containing 4.25 and 6.27 wt% minimum chromium in the depleted grain boundaries respectively. It may be noted that these two samples have the least FWHM of 60 nm also. Figs. 4(a), 7 and 8 indicate that (1) the intragranular carbides had actually contributed less to the reactivation in samples GB1A and GB1D and GB1E i.e. these samples have shallower chromium depletion profiles at the intragranular sites than those at the grain boundaries and (2) the SL-EPR test method used in this study is sensitive down to a minimum chromium level in the depletion regions of 7.5 wt% and saturates below 7.5 wt% chromium. Though the Pa(c) parameter had shown a good overall correlation with the minimum levels of chromium in the depletion regions at grain boundaries (Fig. 4(a)), the modified Pa parameters calculated using Eqs. (4) and (5) provided additional information about the sensitivity of the test and the role of intragranular carbides. The SL-EPR test for type 304 SS had also been reported to be sensitive to minimum chromium in the range from 13 to 7 wt% in the depletion regions [26].

The above analysis using modified Pa parameters showed that the main assumption in calculation of Pa (that all the grain boundaries contribute to the reactivation charge during the EPR test) does not allow a direct correlation of Pa with the minimum level of chromium in the depletion regions. Such a correlation using Pa can be done only in samples where all the grain boundaries are covered with the chromium depletion regions and intragranular carbides are not present. The use of modified Pa parameters (as per Eqs. (4) and (5))

Fig. 7. The Pa(gbc) parameter versus the minimum level of chromium [18] in the depletion regions.

removes the assumptions regarding the reactivation area and intragranular carbides and allows its correlations with the minimum level of chromium in the depletion regions. The electrochemical tests like EPR are sensitive down to a chromium level of 7.5 wt% in the depletion regions as shown in this study and also in an earlier study [26].

4. Conclusions

A single loop EPR test method has been developed for alloy 600. It can be concluded from the present study that

(1) The SL-EPR test method developed in this study results in good passivation on all the surfaces, good etching at the chromium depletion regions and no appreciable pitting. It is able to quantify DOS among samples with different grain boundary chemistry.

(2) The Pa values in the SL-EPR test show a good correlation with the minimum level of chromium in the depletion regions.

(3) The width of the chromium depletion regions has a negative correlation with the Pa values in the SL-EPR test. The volume parameter of the chromium depletion regions does not give any direct correlation with the Pa values in the SL-EPR test.

(4) The width of the attacked regions in the EPR test does not show a direct correlation with either the width, the minimum level of chromium or the volume parameter of the chromium depletion regions. The carbides do not get attacked during the EPR test and the width of the attacked regions is much larger than the width of chromium depletion regions.

(5) The modified Pa parameter (reactivation charge per unit actually attacked grain boundaries) showed a direct indication of the minimum level of chromium in the chromium depletion regions at the grain boundaries down to a level of 7.5 wt%. Below this value of chromium, the modified Pa value tended to saturate and for samples with deeper (and narrow) chromium depletion profiles the modified Pa values decreased. The presence of shallower depletion profiles at the intragranular carbides in samples used in this study could have led to this result.

References

[1] D. VanRooyen, Corrosion 31 (1975) 327.
[2] H.R. Copson, G. Economy, Corrosion 24 (1968) 55.
[3] P.K. De, S.K. Ghosal, Corrosion 37 (1981) 341.
[4] G.P. Airey, Corrosion 35 (1979) 129.
[5] B. Dow Jr., R.C. Thomas, Nucl. Eng. Int. 43 (1998) 38.
[6] A.R. Mcilree, T. Olberg, J. Nestell, in: Steam Generator Reference Book, Chapter 7, Electric Power Research Institute, Palo Alto, CA, 1985.
[7] R. Bandy, D. VanRooyen, Corrosion 40 (1984) 425.
[8] N. Totsuka, E. Lunarska, G. Cragnolino, S. Szklarska-Smialowska, Corrosion 43 (1987) 505.
[9] R. Rios, T. Magnin, D. Noel, O. deBouvier, Metall. Trans. 26A (1995) 925.
[10] T. Cassagne, B. Fleury, F. Vaillant, O. deBouvier, P. Combrade, in: Proceedings of Eighth International Symposium on Environmental Degradation of Materials in Nuclear Power Systems Water Reactors, ANS, 1997.
[11] R.B. Rebak, S. Szklarska-Smialowska, Corros. Sci. 38 (1996) 971.
[12] F.P. Ford, P.L. Andresen, in: Proceedings of Third International Symposium on Environmental Degradation of Materials in Nuclear Power Industries, TMS, 1988.
[13] W.L. Clarke, R.L. Cowan, W.L. Walker, in: R.F. Steiger-wald (Ed.), Intergranular Corrosion of Stainless Alloys, ASTM STP 656, ASTM, Philaladelphia, PA, 1978, p. 99.
[14] S.M. Bruemmer, Mater. Sci. Forum 46 (1989) 309.
[15] D.B. Wells, J. Stewart, A.W. Herbert, P.M. Scot, P.E. Williams, Corrosion 45 (1989) 649.
[16] M.A. Gaudett, J.R. Scully, J. Electrochem. Soc. 140 (1993) 3425.
[17] M.K. Ahn, H.S. Kwon, J.H. Lee, Corrosion 51 (1995) 441.
[18] T.M. Angeliu, E.L. Hall, M.L. Pollick, R. Babler, Corrosion 1999, paper no. 440.
[19] J.L. Hertzberg, G.S. Was, Metall. Mater. Trans. 29A (1998) 1035.
[20] G.S. Was, V.B. Rajan, Corrosion 43 (1987) 576.
[21] R.M. Kruger, S.F. Claeys, G.S. Was, Corrosion 41 (1985) 504.
[22] M.F. Maday, A. Mignon, M. Vittori, Corros. Sci. 28 (1988) 887.
[23] A. Roelandt, J. Vereecken, Corrosion 42 (1986) 289.
[24] S.M. Bruemmer, L.A. Charlott, B.W. Arey, Corrosion 44 (1988) 328.
[25] H. Hanninen, Intergranular Stress Corrosion Cracking, Final Report of the NKA Project MAT 530, VTT, Finland, 1989.
[26] V. Kain, PhD thesis, Indian Institute of Technology, Mumbai, India, 1997.
[27] P. Aaltonen, I. Aho-Mantila, H. Hanninen, Corros. Sci. 23 (1983) 431.
[28] K.N. Adhe, V. Kain, S.S. Chouthai, Indian J. Tech. 28 (1990) 139.